Nonreciprocal Magnons in Noncentrosymmetric Magnets

doi: 10.7566/JPSJ.88.081007

Nonreciprocal Magnons in Noncentrosymmetric Magnets

Taku J Sato[1]* and Kittiwit Matan[2,3,1]

[1]*Institute of Multidisciplinary Research for Advanced Materials, Tohoku University, 2-1-1 Katahira, Aoba, Sendai 980-8577, Japan*

[2]*Department of Physics, Faculty of Science, Mahidol University, Bangkok 10400, Thailand*

[3]*ThEP, Commission of Higher Education, Bangkok 10400, Thailand*

In a noncentrosymmetric crystalline material, the propagation of particles or quasiparticles can be nonreciprocal, *i.e.*, the left-moving and right-moving (quasi)particles become inequivalent. In a noncentrosymmetric magnet, such nonreciprocity is expected for magnons, the quantized collective spin fluctuations that propagate as a wave in a magnetically ordered phase. Even though the nonreciprocal propagation of the magnons was theoretically proposed decades ago, experimentally, little attention has been given to the phenomenon, partly because of its putative subtleness originating from the weak relativistic spin-orbit coupling. The situation has markedly changed recently, as the possibility of measuring and controlling a magnon spin current in noncentrosymmetric magnets begins to gain wider recognition. In this article, we will review recent progress in the detection of the nonreciprocal magnons in noncentrosymmetric magnets. Particular emphasis will be placed on the neutron scattering studies where the magnon dispersion is directly measured in a microscopic length scale.

1. Introduction

Dispersion relations of particles or quasiparticles in solids are crucially related to the symmetry of the underlying crystal structure and have been well classified using group-theory techniques.[1] One of the most celebrated examples of the symmetry effect on the dispersion relation is the Rashba spin splitting of the electronic band structure, which was originally predicted in a noncentrosymmetric bulk semiconductor,[2–5] but was later first confirmed in surface or interfacial two-dimensional electron systems.[6,7] Inevitable symmetry breaking due to the spatial disruption of the surface or interface evokes the Rashba type relativistic spin-orbit coupling, $(\vec{\sigma} \times \vec{k}) \cdot \vec{z}$, where $\vec{k}, \vec{\sigma}$, and $\vec{z}$ are the momentum, spin, and surface-normal vectors,

*taku@tagen.tohoku.ac.jp

respectively. Owing to this Rashba term, electrons with the up- and down-spin states acquire different energies at finite $|\vec{k}|$, resulting in the spin-splitting of the originally degenerated electronic bands. Furthermore, the Rashba coupling locks the spin direction to be perpendicular to its momentum ($\vec{k}$-) direction; this phenomenon is called "spin-momentum" locking.

While the symmetry effect on the electronic band structure is well understood, the subject has recently attracted renewed interest because of its connection to an anomalous transport property. This anomalous transport behavior results from the fictitious magnetic field due to the finite Berry curvature around band crossing points, such as the Dirac and Weyl points, which are expected for crystalline materials with specific symmetry at some particular $\vec{k}$ points.[8,9] An opposite-chirality pair of Weyl nodes act like a monopole and antimonopole in momentum space, which serve as a source and sink for the fictitious magnetic field (Berry curvature flux). The presence of the Weyl nodes could result in the anomalous Hall effect in the electronic transport.[10] The Berry curvature around the Weyl points can also affect magnetic fluctuations. Recent progress in the neutron scattering technique enables the detection of the nonmonotonic temperature dependence of the ferromagnetic spin-wave gap that provides evidence for the effect of the Weyl points on spin dynamics.[11]

The linear crossing of the dispersion relation is ubiquitous for other quasiparticles, including magnons, as it is indeed symmetry-protected. A typical example is the presence of Weyl points in the magnon dispersion that was theoretically proposed in the breathing pyrochlore[12,13] and antiferromagnetic kagome lattices.[14] Experimental observation of the linear crossing and topological magnons, which were measured using neutron inelastic scattering, has been reported for a kagome lattice ferromagnet[15] and recently for a three-dimensional antiferromagnet.[16] A type of anomalous transport behavior that may originate from the magnonic Dirac/Weyl points is of current and growing interest. Noncentrosymmetry is believed to be one of the key ingredients giving rise to the linear crossing in the magnon dispersion, as exemplified by several theoretical studies.[17–19]

Another reason for the growing interest in the particle/quasiparticle dynamics under the noncentrosymmetric environment is the potential for controlling the propagation direction of particles/quasiparticles.[20] One of the most well-known examples is an electronic rectifier. Owing to broken spatial-inversion symmetry at a semiconductor $p-n$ junction, the electronic rectifier allows the unidirectional transport of electrons, making the device a fundamental key component of modern electronics. Such nonreciprocal (unidirectional) propagation can be expected for any particle/quasiparticle in crystalline materials, and is indeed observed for phonons,[21] photons,[22,23] and magnons[24–26] to name a few.

For centrosymmetric crystals, the dispersion relation of spinless particles/quasiparticles in one dimension obeys the symmetry relation $E(k) = E(-k)$. On the other hand, for the noncentrosymmetric crystalline materials, the left- and right-moving particles/quasiparticles can acquire different energies, *i.e.*, $E(k) \neq E(-k)$, and hence the dispersion relation can be asymmetric around the origin $k = 0$. The lowest-order term that brings about such asymmetry is the k-linear term, and the dispersion relation may be rewritten as

$$E(k) = E_0 + D_s(k - k_0)^2, \tag{1}$$

where the bottom of the dispersion relation shifts from the origin to $k = k_0$. The asymmetric dispersion relation is schematically shown in Fig. 1(a). The mechanism for the nonreciprocal propagation of quasiparticles can readily be inferred from the dispersion relation; if we create a quasiparticle (or inject a particle into a bulk noncentrosymmetric material) with a specific energy E and momentum k, then it can only propagate unidirectionally, since at the same energy, the mode that propagates in the opposite direction with momentum $-k$ is absent and hence cannot be excited. This unidirectional propagation was indeed observed using a modern microwave spectroscopy technique as briefly summarized in Sect. 3 of this review. For particles/quasiparticles with a finite spin such as $S = 1/2$, owing to the lack of inversion operation in the SU(2) spin space, the effect of noncentrosymmetry gives rise to the spin-dependent band splitting described by the relations $E(k, \uparrow) = E(-k, \downarrow)$ and $E(k, \downarrow) = E(-k, \uparrow)$, assuming time-reversal symmetry [note that $E(k, \uparrow) \neq E(-k, \uparrow)$ and $E(k, \downarrow) \neq E(-k, \downarrow)$]. This spin-dependent band splitting results in very intriguing nonreciprocal transport in the noncentrosymmetric crystals, in which the propagation is not only unidirectional but also spin-dependent.

In this review, we will not try to cover the broad subject of nonreciprocal responses, which has been comprehensively reviewed in Ref. 27, but instead will focus on the nontrivial dispersion of magnons in both ferromagnets and antiferromagnets, and its consequences on nonreciprocal transport. In Sect. 2, we will summarize the expected symmetry effects on the magnon dispersion in a simple collinear one-dimensional ferromagnet and antiferromagnet. The detection of the nonreciprocal magnons with microwave technology is overviewed in Sect. 3, whereas the recent results and complete characterization of the dispersion relation in a noncentrosymmetric ferromagnet and antiferromagnet will be given in Sect. 4. In Sect. 5, the future prospects of nonreciprocal magnons are discussed, and Sect. 6 concludes this article.

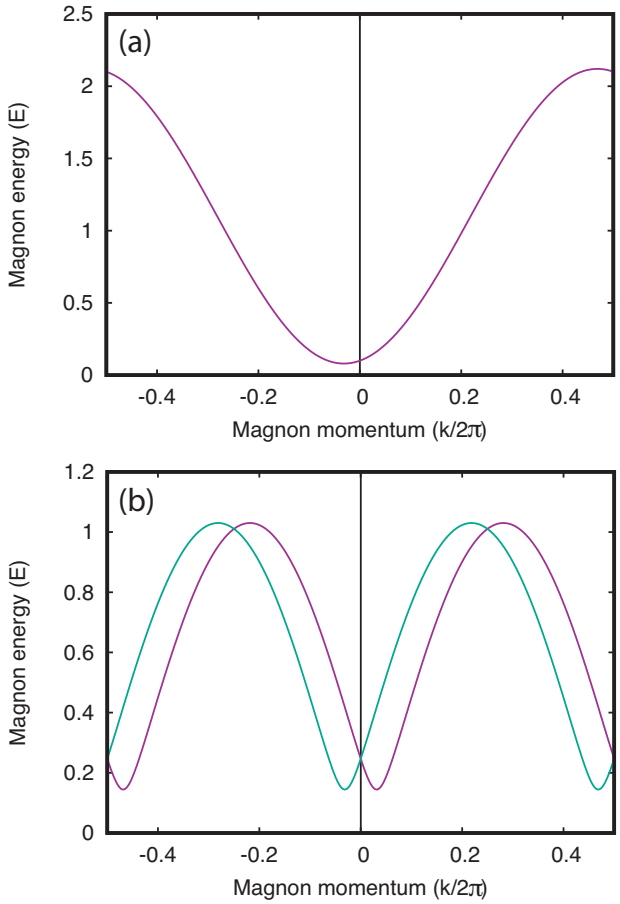

Fig. 1. (Color online) Schematical illustrations of magnon dispersion relations in (a) noncentrosymmetric ferromagnet and (b) noncentrosymmetric antiferromagnet. The Hamiltonian parameters $S = 1/2, J = -1, D^z_{\rm DM} = 0.2$, and $D = -0.1$ are used for (a). The same parameter set except for $J = 1$ and $D = -0.03$ was used for (b). The lattice constant is set to $d = 1$.

2. Noncentrosymmery and Dispersion Relation of Magnons

In this section, we will give a brief summary of the magnon dispersion relations in noncentrosymmetric magnets by considering simple models of a collinear one-dimensional ferromagnet and antiferromagnet in the large-spin-size (S) limit. Noted that elaborate treatments of magnons in various noncentrosymmetric magnets have been given in a number of publications to date.[17,28–31] When the inversion symmetry is absent around the midpoint of a bond connecting two interacting spins in a magnetic material, the antisymmetric spin-spin interaction of the relativistic spin-orbit-coupling origin or Dzyaloshinskii–Moriya (DM) interaction becomes activated. As a result, a simple spin Hamiltonian for a one-dimensional

noncentrosymmetric Heisenberg magnet shown in Fig. 2 may be given as

$$\mathcal{H} = \sum_{<i,j>} \left[J_{ij} \vec{S}_i \cdot \vec{S}_j + \vec{D}_{\mathrm{DM}ij} (\vec{S}_i \times \vec{S}_j) \right] + \sum_i D (S_i^z)^2, \tag{2}$$

where $\vec{S}_i (\vec{S}_j)$ is the spin operator at the $i(j)$-site and $J_{ij} (\vec{D}_{\mathrm{DM}ij})$ is the isotropic (antisymmetric) interaction parameter. J, which is negative for a ferromagnet and positive for an antiferromagnet, and $\vec{D}_{\mathrm{DM}}$ (denoted by green arrows in Fig. 2) are assumed to be uniform, so that their suffixes are neglected. The summation is to be performed for the nearest-neighbor pairs along a one-dimensional chain. The single-site anisotropy term $D(S_i^z)^2$ aligns the spins along the quantization axis (the z-axis) and induces the collinear ordered structure. It may be noted here that in an $S = 1/2$ system, such as α-$Cu_2V_2O_7$ discussed later, the single-ion-type anisotropy vanishes, and exchange interaction anisotropy becomes effective instead. For the dominant ferromagnetic spin-spin interaction with a sufficiently weak easy axis anisotropy and DM interaction ($|J| >> |D|$ and $|\vec{D}_{\mathrm{DM}}|$ with sufficiently large and negative D), the ground state becomes a fully polarized ferromagnetic state with $\langle \vec{S}_i \rangle = (0, 0, +S)$, independent of the site i as shown in Fig. 2(a). Similarly, for the antiferromagnet, the classical ground state is the two-spin-sublattice collinear Néel state with $\langle \vec{S}_i \rangle = (0, 0, \pm S)$ as shown in Fig. 2(b).

For the ferromagnet, the low-energy spin excitations from the ground state may be obtained by linearizing the above Hamiltonian [Eq. (2)] using the well-known Holstein–Primakoff transformation and taking the lowest order of the boson operators; the result can be written as

$$\mathcal{H} = E_0 + \sum_k \vec{X}_k^\dagger H(k) \vec{X}_k, \tag{3}$$

where $\vec{X}_k^\dagger = (a_k^\dagger, a_{-k})$, and the k-dependent quadratic Hamiltonian matrix is given by

$$H(k) = \begin{pmatrix} \omega_k & 0 \\ 0 & \omega_{-k} \end{pmatrix}, \tag{4}$$

where $\omega_k = 2S\ (c_k - J + s_k - D)$, $c_k = J\cos(kd)$, $s_k = D^z_{\mathrm{DM}} \sin(kd)$, and d denotes the lattice constant. It is assumed for clarity that $\vec{D}_{DM} = (0, 0, D^z_{DM})$ since the x- and y-components of the DM vector do not contribute to the shift of the dispersion. The dispersion relation is illustrated in Fig. 1(a). Owing to the finite DM interaction, the bottom of the magnon dispersion shifts away from the origin. In the long-wavelength limit, it is apparent that the magnons propagating in the $+k$ and $-k$ directions have different group velocities, which are defined by the slope of $E(k)$; therefore, the magnon propagation is nonreciprocal.

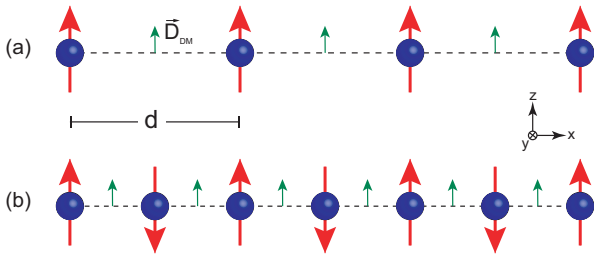

Fig. 2. (Color online) Spin models for the one-dimensional (a) ferromagnetic and (b) antiferromagnetic chain with uniform DM interactions. The red (longer) arrows indicate directions of spin ordering, whereas the green (shorter) ones denote the DM vectors.

For the antiferromagnetic Néel state, the two sublattices give rise to two kinds of magnon operators, $a_{0,k}$ and $a_{1,k}$. Consequently, the basis vector can be represented by $\vec{X}_k^\dagger = (a_{0,k}^\dagger, a_{1,k}^\dagger, a_{0,-k}, a_{1,-k})$, and the quadratic Hamiltonian matrix now reads

$$H(k) = 2S \begin{pmatrix} J-D & 0 & 0 & -(c_k+s_k) \\ 0 & J-D & -(c_k-s_k) & 0 \\ 0 & -(c_k-s_k) & J-D & 0 \\ -(c_k+s_k) & 0 & 0 & J-D \end{pmatrix}. \tag{5}$$

In contrast to the trivial ferromagnetic order, off-diagonal terms appear, *e.g.*, $a_{0,k}^\dagger a_{1,-k}^\dagger$, through which the DM interaction gives rise to the antisymmetric contribution in terms of $\sin(kd)$. To acquire a diagonal form of the Hamiltonian matrix with bosonic quasiparticles, the Bogoliubov transformation may be performed by introducing a matrix T_k, which transforms $\vec{X}_k$ to new boson operators $\vec{Y}_k$ with $\vec{Y}_k = T_k \vec{X}_k$. T_k should satisfy the boson condition $T_k \Gamma T_k^\dagger = \Gamma$, where

$$\Gamma = \begin{pmatrix} 1 & 0 & 0 & 0 \\ 0 & 1 & 0 & 0 \\ 0 & 0 & -1 & 0 \\ 0 & 0 & 0 & -1 \end{pmatrix}, \tag{6}$$

and the diagonalization condition

$$T_k^{-1} \Gamma H(k) T_k = \frac{1}{2} \Gamma \Omega_k. \tag{7}$$

Using T_k given above, the Hamiltonian is diagonalized as $\vec{X}_k^\dagger H(k)\vec{X}_k = \vec{Y}_k^\dagger \frac{1}{2}\Gamma\Omega_k\vec{Y}_k$, where

$$\Omega_k = \begin{pmatrix} \omega_{+,k} & 0 & 0 & 0 \\ 0 & \omega_{-,k} & 0 & 0 \\ 0 & 0 & \omega_{+,-k} & 0 \\ 0 & 0 & 0 & \omega_{-,-k} \end{pmatrix}. \tag{8}$$

The obtained eigenenergies are given by

$$\omega_{\pm,k} = 2S\sqrt{(J-D)^2 - (c_k \pm s_k)^2}. \tag{9}$$

This dispersion relation is schematically illustrated in Fig. 1(b). Owing to the finite DM interaction, the two originally degenerated magnon bands shift in the $-k$ and $+k$ directions, giving rise to a linear crossing at $k = 0$. Noted that owing to the linear dispersion of the antiferromagnetic magnons in the small-k region and the symmetric appearance of the two branches of the dispersion around the origin, the group velocities of the $\pm k$ modes are identical. Nonetheless, since the two modes, which are split by the DM interactions, correspond to different spin dynamics with opposite rotations (*i.e.*, clockwise and counterclockwise), by selectively exciting a single mode, the nonreciprocity of the phase velocity can be achieved. Note further that at the crossing, the spin dynamics change the spin rotation from clockwise to counterclockwise or vice versa. The counter-rotating spin dynamics may be regarded as a spin variable with opposite signs (*i.e.*, positive for counterclockwise and negative for clockwise), and hence at $k = 0$ where the linear crossing occurs, this spin variable changes its sign. This spin-dependent dispersion relation illustrates one of the simplest examples of the "spin-momentum locking" in a magnonic system, the general treatments of which may be found in recent theoretical studies.[18,19]

3. Microwave Detection of Nonreciprocal Propagation of Magnons

In ferromagnetic thin films, long-wavelength spin waves predominantly propagate via the long-range dipolar interaction. In such a long-wavelength region, nonreciprocal propagation was proposed for surface magnetostatic modes decades ago, which is now called the Damon–Eshbach mode.[32] The Damon–Eshbach mode on one surface propagates unidirectionally, as experimentally confirmed in an $Y_3Fe_5O_{12}$ film using microwave spectroscopy,[33] indicating the nonreciprocal flow of the magnon spin current. However, counter-propagating modes exist on the opposite surface of the film, and consequently, the spin currents cancel each other out; therefore, the net magnon spin current vanishes. In order to realize a non-zero bulk magnon spin current, it is necessary to inhomogeneously (or selectively) excite the two surface modes,

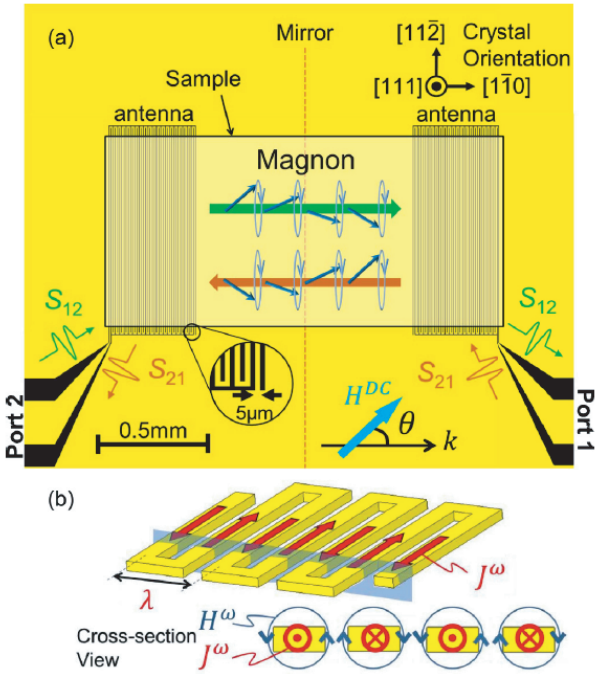

Fig. 3. (Color online) (a) Configuration of microwave spectroscopy for the detection of nonreciprocal magnons in the noncentrosymmetric ferromagnet $LiFe_5O_8$. Meander antennae are placed under a rectangularly cut $LiFe_5O_8$ sample. (b) Spatially oscillating magnetic fields induced by the meander antenna. Reprinted with permission from Ref. 24. Copyright (2015) by the American Physical Society.

so that the magnon spin currents on the opposite sides of the film do not completely negate each other. The generation of thermal gradient due to the bulk magnon spin current induced by inhomogeneous Damon–Eshbach modes has recently been confirmed.[34]

The nonreciprocal Damon–Eshbach mode originates from a purely macroscopic shape effect, and is explained using the Maxwell equations and equation of motion for macroscopic magnetization. On the other hand, trivial inversion-symmetry breaking at the surfaces or interfaces will induce microscopic DM interactions between spins in the surface or interface region. Hence, nonreciprocity due to the finite DM interaction should appear, in addition to that originating from the Damon–Eshbach mechanism. Indeed, the asymmetric magnon dispersion due to the surface/interface DM interaction has been directly observed in an Fe double layer grown on a W(110) substrate using spin-polarized electron energy loss (SPEEL) spectroscopy,[35] and in Pt/Co/Ni multilayers using Brillouin light scattering spectroscopy,[36] to name a few.

Similar to a surface and interface, bulk noncentrosymmetry may induce the nonreciprocal propagation of magnons. Advantageously, bulk nonreciprocal magnons may generate

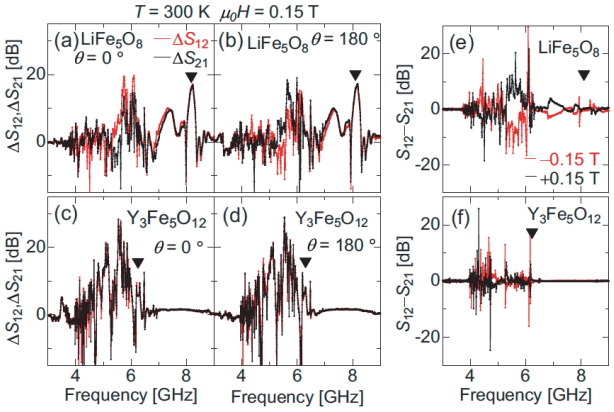

Fig. 4. (Color online) (a-d) Transmittance of microwave owing to the magnon propagation from left to right (ΔS_{12}) and right to left (ΔS_{21}). To show the magnon transmittance, the difference from the 1.0 T data is shown as ΔS. (e) and (f) Difference of transmittance between the two magnetization directions. The samples are (a, b, e) the noncentrosymmetric ferromagnet $LiFe_5O_8$ and (c, d, f) centrosymmetric $Y_3Fe_5O_{12}$. Reprinted permission from Ref. 24. Copyright (2015) by the American Physical Society.

nonzero net magnon spin current in a ferromagnet with the uniform DM interaction since the nonreciprocity of the magnon dispersion in this system is uniform throughout the sample, giving rise to a unidirectional magnon spin current. In order to investigate these bulk nonreciprocal magnons, quite a few microwave spectroscopy measurements have been performed on the noncentrosymmetric magnets recently. Iguchi *et al.* first observed bulk nonreciprocal magnon propagation using the archetypal noncentrosymmetric ferromagnet $LiFe_5O_8$,[24] which crystallizes in the cubic space group $P4_132$.[37] This compound shows collinear ferrimagnetic order below 900 K.[38] In order to measure the magnon propagation at a finite k-vector, they fabricated meander microwave antennae on the left and right sides of the sample front surface (Fig. 3) and measured the transmittance of the magnon signals in both directions. The data [Figs. 4(a), 4(b), and 4(e)] show the difference in the transmittance, which indeed depends on the direction of the net magnetization controlled by the external magnetic field. In contrast, the dependence of the transmittance on the magnetization direction was not observed in the centrosymmetric $Y_3Fe_5O_{12}$ [Figs. 4(c), 4(b), and 4(f)]. The authors thus conclude that in a noncentrosymmetric ferromagnet, the magnon propagation is nonreciprocal and controllable by the external magnetic field.

In another work, Seki *et al.* implemented almost the same experimental configuration to measure the nonreciprocal magnons in the chiral insulating compound Cu_2OSeO_3,[25] which belongs to the cubic space group $P2_13$.[39,40] This compound has a helically ordered state below

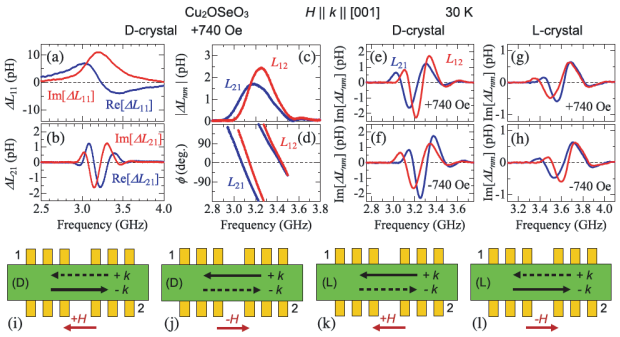

Fig. 5. (Color online) Inductance spectrum ΔL_{nm} for Cu_2OSeO_3. Spinwave contribution at $H = 740$ Oe (polarized ferromagnetic state), estimated as the difference from the high-field inductance measured at $H = 2650$ Oe. (a) and (b) Real and imaginary parts of self-inductance and mutual inductance. (c) and (d) magnitude and phase of mutual inductance, respectively. (e-h) Comparison between D- and L-crystals. (i-l) Experimental setups used in the measurement. Reprinted with permission from Ref. 25. Copyright (2016) by the American Physical Society.

$T_c \sim 59$ K, and also hosts an intriguing magnetic skyrmion phase under a weak external magnetic field.[41] For the observation of the nonreciprocal magnons, they applied an external magnetic field of $H = 740$ Oe parallel/antiparallel to the magnon propagation direction to induce a uniformly magnetized state. The microwave excitation was provided by coplanar waveguides fabricated on an oxidized silicon substrate, and a Cu_2OSeO_3 film was placed on top of the waveguides. The measured self-inductance L_{11} [Fig. 5(a)] represents the efficiency of the magnon excitations, and the mutual inductance L_{12} or L_{21} [Fig. 5(b)] provides valuable information about the magnon propagation direction between two ports labeled by 1 and 2 shown in Figs. 5(i-l). The difference between L_{12} and L_{21} shown in Fig. 5(c) indicates the magnon contribution to the mutual inductance and more importantly provides evidence for nonreciprocal magnons in Cu_2OSeO_3. The advantage of this experiment is that the chirality of the crystal used in the measurements can be controlled. It can be seen from the results [Fig. 5(e-h)] that the magnon contribution has the opposite effect on the mutual inductance of the right-handed (D) and left-handed (L) crystals, which have opposite chiralities, confirming that the chirality is a dominant deterministic factor of the magnon propagation direction.

As seen from the above two examples, spinwave spectroscopy provides a novel method to characterize the DM interaction and nonreciprocal magnons in chiral or noncentrosymmetric magnets, and research activities along this line continue to date.[26] The recent work of Seki *et al.* has been extended to the detection of nonreciprocal magnons in the skyrmion phase. This work leads to an interesting observation on the interconnecting nature of the topolog-

ical spin texture and magnon propagation, the details of which can be found in the original manuscript.[42]

4. Direct Observation of Asymmetric Dispersion Relations of Magnons by Inelastic Neutron Scattering

It is clear from modern microwave spectroscopy measurements that magnons in the bulk noncentrosymmetric magnets propagate nonreciprocally. Nonetheless, these microwave spectroscopy measurements have a few drawbacks that require further experimental investigations. First, these experiments are carried out in a low-energy (GHz) region where the dipolar interaction is dominant.[43] In such an energy range, the magnon group velocity is negative, and the effect of the bulk DM interaction is indeed supplemental. Secondly, the wavelength of the magnons excited in the microwave spectroscopy experiments is fixed by the antenna design. Hence, it is difficult to measure the wavelength (or k-) dependence of the magnon dispersion. Since the precise measurement of the magnon dispersion is a key to confirming its asymmetric shift due to the noncentrosymmetry and to quantitatively estimate the exchange and DM parameters in the bulk, it is strongly desirable to directly measure the dispersion relation. In addition, such microwave spectroscopy has only been performed in noncentrosymmetric ferromagnets to date. Investigation on the noncentrosymmetric antiferromagnets has been largely unexplored, since for long-wavelength ($k \sim 0$) microwaves, antiferromagnetic magnons cannot be excited in the experimentally reachable energy range using microwave network analyzers. A high-frequency (sub-THz) electron-spin resonance experiment may be one possibility, but the k dependence measurement seems to be difficult. Hence, for antiferromagnetic magnons, neutron inelastic scattering is the only practical tool that can be used to obtain the dispersion relations. In this section, we will review recent studies of the asymmetric dispersion relations in noncentrosymmetric magnets using the inelastic neutron scattering technique. Focus will be given to the two archetypal noncentrosymmetric magnets: the celebrated itinerant chiral magnet MnSi and the relatively new noncentrosymmetric antiferromagnet α-$Cu_2V_2O_7$.

4.1 Itinerant noncentrosymmetric ferromagnet MnSi

The first direct observation of an asymmetric magnon dispersion using inelastic neutron scattering was carried out on the prototypical itinerant chiral magnet MnSi. This compound has been of considerable interest for almost half a century and is now attracting renewed interest because of the discovery of an intriguing skyrmion-lattice phase under finite magnetic

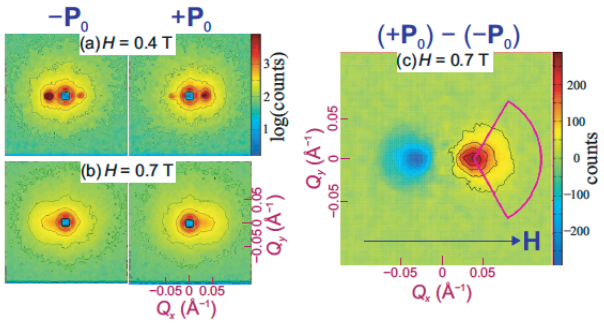

Fig. 6. (Color online) (a) and (b) Polarized-neutron small-angle scattering results for MnSi under magnetic field (a) $H = 0.4$ T (conical) and (b) $H = 0.7$ T (fully polarized) observed at $T = 15$ K. (c) Intensity difference between the $+\vec{P}_0$ and $-\vec{P}_0$ polarization directions of the incident neutrons. Reprinted with permission from Ref. 50. Copyright (2015) by the American Physical Society.

field and temperature.[44] MnSi crystallizes in the space group $P2_13$; the crystal structure is noncentrosymmetric and chiral. Under zero external magnetic field, MnSi exhibits long-range helical magnetic order at $T_c \sim 29.5$ K, with the long-wavelength modulation characterized by the modulation vector $\vec{q} \sim (0.016, 0.016, 0.016)$ (r.l.u.).[45,46] The single-$\vec{q}$ helical structure transforms into a conical structure under a finite magnetic field. Then, with a sufficiently large external field ($H > 6000$ Oe at base temperature), the field-induced ferromagnetic phase (or fully polarized state) is stabilized.[47]

The asymmetric magnon dispersion was predicted theoretically for this compound based on its microscopic model Hamiltonian,[29] as well as more generally on the symmetry argument.[28] Experimentally, there have been two pioneering works on the detection of the magnon-dispersion asymmetry in this compound. Both of them used the polarization analysis of inelastic thermal-neutron scattering. One reported that the ferromagnetic magnon excitation spectrum becomes asymmetric for $\pm\vec{k}$ when the magnons with clockwise and counterclockwise rotations were separately observed using the polarization analysis,[48] whereas the other observed the change in the magnon peak position by reversing the external magnetic field direction (*i.e.*, magnetization direction).[49] Although these observations suggest the asymmetric dispersion relation of the ferromagnetic magnons in MnSi, the limited Q and $\hbar\omega$ resolutions of the available spectrometers at the time of the experiments prohibited them from directly observing the whole dispersion relation curve. This situation has changed with current state-of-the-art neutron spectrometers.

Recently, the asymmetry of the magnon dispersion has been further investigated using polarized neutron small-angle scattering (SANS).[50] As a result of the small gap energy E_g

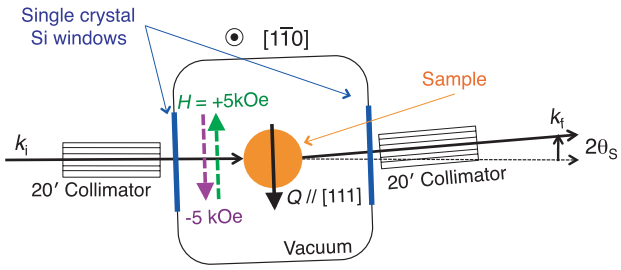

Fig. 7. (Color online) Experimental setup for the detection of the ferromagnetic magnon dispersion shift in the vicinity of $\vec{Q} \sim 0$ using the cold-neutron triple-axis spectrometer CTAX. The momentum transfer $\vec{Q}$ was set along the crystallographic [111] axis. The external magnetic field was fixed either antiparallel ($H > 0$) or parallel ($H < 0$) to $\vec{Q}$. From Ref. 51.

of the ferromagnetic magnons in MnSi, the magnon dispersion bottom is close to the elastic channel, hindering the direct detection, and hence polarized neutrons were utilized. At a sufficiently high temperature compared with the gap energy ($k_BT \gg E_g$), both neutron-energy-loss and neutron-energy-gain scattering processes are almost equally likely, resulting in two similar-intensity peaks at positive ($\hbar\omega > 0$) and negative ($\hbar\omega < 0$) energy transfer. For the asymmetric magnon dispersion [Fig. 1(a)], the magnon dispersion bottom is located at finite $\vec{k}$, and hence the positive-energy magnons (shifted to $-\vec{k}$) have the opposite rotation direction from the negative-energy magnons that are shifted to $+\vec{k}$ (not shown). Using polarized neutrons to distinguish the rotation direction of the spin precession, Grigoriev *et al.*[50] succeeded in separately observing the positive-energy and negative-energy branches of the asymmetric magnons in MnSi without energy analysis. Figures. 6(a) and 6(b) show the results of the polarized neutron small-angle scattering measurements in the conical ($\mu_0 H = 0.4$ T) and fully polarized ($\mu_0 H = 0.7$ T) states in MnSi. By reversing the incident neutron polarization P_0, they showed that the maximum of the scattering intensity moves from the right ($-\vec{P}_0$) to the left ($\vec{P}_0$) side of the origin. The difference in the scattering intensity between the two polarization states is shown in Fig. 6(c). For a given polarization state of the incident neutrons, one side of the origin shows a higher scattering intensity than the other side, indicating that the positive- and negative-energy branches with the bottoms at $-\vec{k}$ and $+\vec{k}$, respectively, correspond to the spin dynamics with the opposite rotation. This result, although indirectly, confirms the asymmetric shift of the magnon dispersion in the noncentrosymmetric chiral MnSi.

Direct measurements of the magnon dispersion in MnSi in the low-energy region have been recently performed by one of us using small-angle inelastic neutron scattering.[51] In

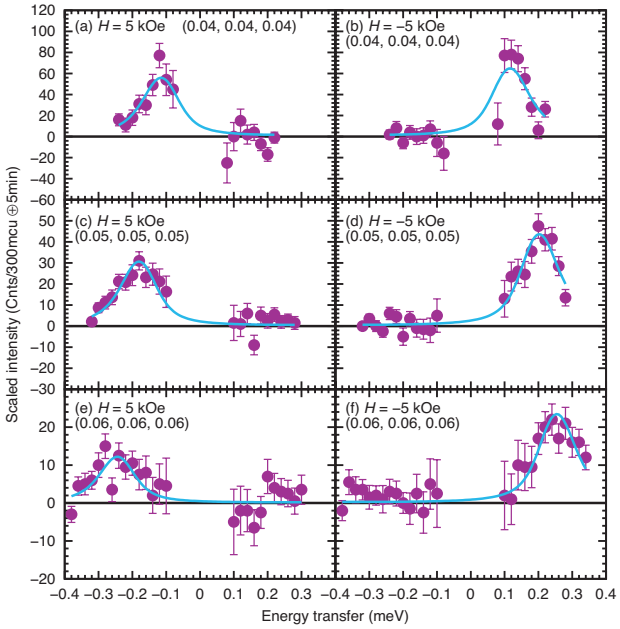

Fig. 8. (Color online) Representative constant-$\vec{Q}$ scans measured at $T = 27$ K. (a) and (b) $h = 0.04$ (r.l.u.); (c) and (d) $h = 0.05$ (r.l.u.); (e) and (f) $h = 0.06$ (r.l.u.). The external field was $H = 5$ kOe for (a, c, e), and $H = -5$ kOe for (b, d, f). The background was removed using the base temperature data. The solid lines are the results of a resolution-convoluted fitting to the intrinsic Lorentzian type peak function. From Ref. 51.

this experiment, to realize sufficiently high Q and $\hbar\omega$ resolutions, a tight collimation setup with a cold-neutron triple-axis spectrometer was employed. The combination of the long-wavelength cold neutrons and tight collimations before and after the sample shown in Fig. 7 enabled us to achieve high Q and $\hbar\omega$ resolutions, $\Delta Q \simeq 0.01$ Å^{-1} and $\Delta\hbar\omega \simeq 0.1$ meV.

The inelastic scattering spectra obtained at $T = 27$ K under the external magnetic field $H = 5$ kOe parallel and antiparallel to the momentum transfer are shown in Fig. 8. Exemplified by the spectrum at $\vec{Q} = (0.05, 0.05, 0.05)$ (r.l.u.) under $H = 5$ kOe, one observes the inelastic magnon peak only in the negative-energy region ($\hbar\omega < 0$), where neutrons gain energy from the system. If one reverses the external magnetic field direction to $H = -5$ kOe, then the inelastic peak appears only in the positive-energy region ($\hbar\omega > 0$). The spectra observed at different $\vec{Q}$ positions exhibit qualitatively identical behavior, confirming that this asymmetric spin-dynamics is common to all $\vec{k}$-vectors.

The detailed balance law for the neutron inelastic scattering function is given by

$$S(\vec{Q}, \hbar\omega) = \mathrm{e}^{\hbar\omega/k_{\mathrm{B}}T} S(-\vec{Q}, -\hbar\omega), \tag{10}$$

where k_{B} is the Boltzmann constant. At $T = 27$ K and for the low-energy range of the present observation ($\hbar\omega < 0.4$ meV ~ 5 K), the temperature factor is almost unity as $\mathrm{e}^{\hbar\omega/k_{\mathrm{B}}T} \simeq$

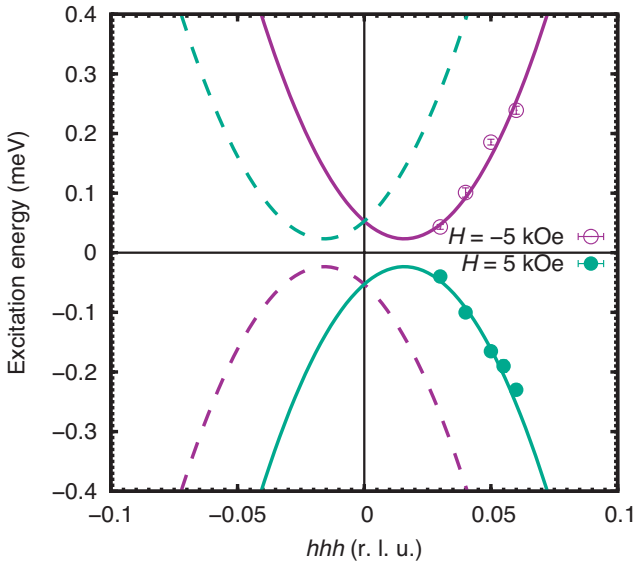

Fig. 9. (Color online) Experimentally obtained magnon dispersion in the low-$\vec{Q}$ region in the induced ferromagnetic state of MnSi. The open circles are for $H = -5$ kOe, whereas filled ones for $H = 5$ kOe. The solid lines are expected quadratic dispersion relations, whereas the dashed lines are counterparts to the solid lines that was not observed in the experiment. From Ref. 51.

1. For the centrosymmetric case where $\vec{Q}$ and $-\vec{Q}$ are equivalent $S(\vec{Q}, \hbar\omega) \simeq S(\vec{Q}, -\hbar\omega)$. Hence, in centrosymmetric magnets, a constant-Q scan will show two inelastic peaks that are symmetrically located around $\hbar\omega = 0$ at positive and negative energies. On the other hand, for the noncentrosymmetric case, where $\vec{Q}$ and $-\vec{Q}$ become inequivalent, this is not necessarily the case, that is, the positive-energy and negative-energy peaks may not appear symmetrically around $\hbar\omega = 0$. The latter is consistent with our observation of the magnon dispersion in MnSi, where one observes only a single peak appearing at either positive or negative energy depending on the external magnetic field direction. More specifically, for the shifted magnon dispersion expected for a noncentrosymmetric ferromagnet shown in Fig. 1(a), according to Eq. (10), the spinwave excitation energies for $\hbar\omega > 0$ and $\hbar\omega < 0$ differ, since they correspond to the $-\vec{k}$ and $+\vec{k}$ modes, respectively; for the magnon excitation at a given energy $\hbar\omega_0$ and momentum $\vec{k}$, its counterpart on the negative-energy side $-\hbar\omega_0$ is not observed at $\vec{k}$ but instead at $-\vec{k}$. In other words, the asymmetric appearance of the magnon excitation spectrum is direct confirmation of the asymmetric magnon dispersion shift in MnSi.

The experimentally deduced dispersion relation using the estimated magnon energies measured at several $\vec{Q}$ positions is shown in Fig. 9. For the negative magnetic field $H = -5$ kOe, which is parallel to the momentum transfer direction, the magnon dispersion is clearly shifted to a positive momentum transfer. Owing to the limitation of the experiment,

a sufficiently low-$\vec{Q}$ region for the complete measurement of the dispersion is not reachable. Therefore, only the magnon dispersion on the $+\vec{Q}$-side, which shows the expected quadratic behavior for a ferromagnet, was observed. Nevertheless, it is clear that the observed magnon peak positions are in perfect agreement with the shifted magnon dispersion given in Eq. (1) as shown by the purple line in Fig. 9. When the magnetic field is reversed to $H = +5$ kOe, the dispersion shift appears in the opposite direction, and thus the positive-energy magnon, which would appear at an energy beyond the range of the measurements, was not observed. In contrast, its counterpart on the negative-energy side, which appears within the measuring range, can be observed and shows the same quadratic behavior (the green line in Fig. 9). Taking into account the detailed balance law for noncentrosymmetric magnets, Eq. (10), this result is consistent with the shifted asymmetric dispersion relation, with which the shift direction is determined by the relationship between the DM interaction and magnetization direction. Since the magnetization direction for the fully polarized ferromagnetic state can be controlled by the external field, this result indicates that the magnon propagation direction can be controlled by the external magnetic field. Further neutron-scattering studies on nonreciprocal magnon dispersions in a wider external field range have been recently reported.[52,53]

4.2 Insulating noncentrosymmetric antiferromagnet α-$Cu_2V_2O_7$

Noncentrosymmetric antiferromagnets have been less explored in terms of the nonreciprocity of the magnon propagation to date, probably because microwave spectroscopy, which has been widely and successfully used for ferromagnetic materials, cannot be easily applied to antiferromagnets, as noted earlier. Neutron inelastic scattering, on the other hand, has no fundamental restriction on exciting finite-$\vec{Q}$ magnons, and hence is an ideal tool capable of observing magnons in noncentrosymmetric antiferromagnets. The first confirmation of the magnon dispersion shift in the noncentrosymmetric antiferromagnets has been recently reported for the noncentrosymmetric antiferromagnet α-$Cu_2V_2O_7$.[54] This compound belongs to the orthorhombic space group $Fdd2$,[55,56] and only the Cu^{2+} ions are magnetically active with $S = 1/2$, whereas V^{5+} is nonmagnetic. Below $T_N = 33.4$ K, the $S = 1/2$ Cu^{2+} spins form a nearly collinear antiferromagnetically ordered state with the dominant magnetic-moment component along the crystallographic a-axis as a result of the anisotropic exchange interaction.[57,58] In addition, the DM interaction gives rise to the field-induced canting of the ordered moment and weak ferromagnetism below T_N when an external magnetic field is applied along the c-axis. However, since the field-induced spin canting is small, estimated to be as small as 4.0° in the small-field limit,[59] the ordered magnetic structure at zero field is

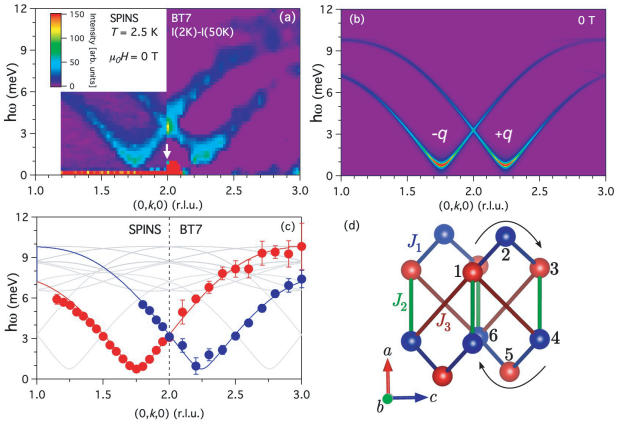

Fig. 10. (Color online) (a) Magnetic scattering intensity map for α-$Cu_2V_2O_7$. For the BT7 data, the scattering intensity was obtained by subtracting the paramagnetic data at $T = 50$ K from the base temperature $T = 2$ K data. (b) Scattering intensity calculated using the linear spinwave theory with the 16-sublattice model described in the text. Only two branches can be seen due to the negligible structure factor for the other branches. (c) Experimentally determined dispersion relations with the calculated ones. The gray lines denote the almost invisible spinwave branches. (d) Spin network of α-$Cu_2V_2O_7$ with the dominant exchange interactions J_1, J_2, and J_3. The red and blue spheres stand for the two sublattices with opposite spin directions. From Ref. 54.

assumed to be collinear, ignoring the weak ferromagnetic component.

Figure 10 shows a map of the magnetic scattering intensity a function of energy transfer and momentum transfer obtained by subtracting the paramagnetic background ($T = 50$ K) from the base temperature data at $T = 2$ K. The data was taken along the $\vec{b}^*$-direction around the $\vec{Q} = (0, 2, 0)$ reflection, where the magnetic Bragg peak from the collinear antiferromagnetic ordering appears. The result [Fig. 10(a)] clearly shows two magnon branches in the excitation spectrum and a linear crossing of the two branches at the antiferromagnetic zone center. This magnon dispersion shift is indeed due to the DM interaction expected in the two-sublattice antiferromagnetic model described in Sect. 2 [Fig. 1(b)]. As a result of the DM interaction, two originally degenerate modes with opposite rotation (precession) split into two nondegenerate modes and symmetrically shift to $+q$ and $-q$ [Fig. 10(b)], where $\pm q$ denotes the momentum transfer along the $\vec{b}^*$-direction measured from (0, 2, 0). The small but finite gap in the excitation spectrum was estimated to be $\Delta = 0.75(6)$ meV using a high-energy-resolution triple-axis spectrometer. This spinwave gap indicates that sufficiently strong easy-axis-type anisotropy fixes the magnetic structure to be collinear and overwhelms the effect of the DM interaction, which prefers a helical magnetic structure. In other words, the static ordered state due to the anisotropic interaction, which is more dominant than the DM interaction, gives rise to commensurate Bragg peaks, whereas incommensurability due to the DM

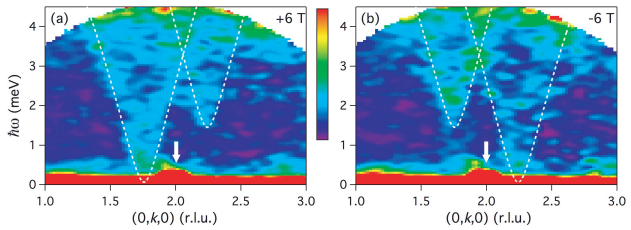

Fig. 11. (Color online) (a-b) Magnetic scattering intensity maps for α-$Cu_2V_2O_7$ in applied external magnetic field. The external magnetic field along the a-axis was applied with (a) $H = +60$ kOe and (b) $H = -60$ kOe. The dashed lines denote the most intense branches of the calculated spinwaves. From Ref. 54.

interaction only appears in the fluctuating part of the spin dynamics, and hence in the inelastic response.

The external magnetic field affects and modifies the magnon dispersion in an interesting manner. The magnetic scattering spectra under an external field of $H = \pm 60$ kOe are shown in Fig. 11. The magnetic field was applied in the vertical direction and along the crystallographic a-axis, along which the dominant component of magnetic moments aligns. For the positive magnetic field $H = 60$ kOe, the branch that has the dispersion minimum on the $-q$ side decreases in energy, whereas the energy of the other branch increases. In contrast, for the negative magnetic field $H = -60$ kOe, the energy of the $+q$ branch decreases, whereas that of the $-q$ branch increases. This field dependence of the excitation energy clearly indicates the opposite precession of the spin dynamics corresponding to the two branches. It is noteworthy that this external-field dependence of the magnon dispersion is similar to that of the Rashba split electron bands, where the Zeeman energy gives rise to the opposite response for the up- and down-spin bands of electrons. The relationship between this observation for the antiferromagnetic magnons and the electronic band structure will be further discussed in Sect. 6.

Although the essence of the magnon dispersion shift is captured by the simple two-sublattice antiferromagnetic spin model with the uniform DM interactions discussed in Sect. 2, the reality in α-$Cu_2V_2O_7$ is far from such a simple model. Indeed, combined density functional theory (DFT) calculations and quantum Monte Carlo simulations suggest a complex spin-interaction network, which can be given to the first approximation as

$$\begin{aligned} \mathcal{H} &= \sum_{i,j} J_{ij} \vec{S}_i \cdot \vec{S}_j + \sum_{k,l} G_{kl} (S_k^x S_l^x - S_k^y S_l^y - S_k^z S_l^z) \\ &+ \sum_{k,l} \vec{D}_{kl} \cdot (\vec{S}_k \times \vec{S}_l) - g\mu_B \sum_i \vec{S}_i \cdot \vec{H}, \end{aligned} \tag{11}$$

where the summation $\sum_{i,j}\left(\sum_{k,l}\right)$ is taken over the nearest, next-nearest, and third-nearest neighbors (nearest neighbors), and $\vec{H}$ denotes the external magnetic field. The ratio of the nearest, next-nearest, and third-nearest neighbor isotropic exchange parameters, which we redefine as J_1, J_2, and J_3, was estimated by the DFT calculations as $J_1 : J_2 : J_3 = 1.00 : 1.12 : 2.03$.[60] For the sake of simplicity, the anisotropic exchange and DM interactions are assumed for the nearest neighbors. Furthermore, from the crystal symmetry and the observed shift direction of the magnon dispersion, the DM interaction was assumed to be along the a-axis as $\vec{D} = (D_{1a}, 0, 0)$. With the above assumptions and simplification, the observed magnon dispersion relations are satisfactorily reproduced using the parameters $J_1 = 2.67(1)$ meV, $J_2 = 2.99$ meV, $J_3 = 5.42$ meV, $G_1 = 0.282(1)$ meV, and $D_{1a} = 2.79(1)$ meV. The resulting calculated magnon dispersion is shown in Fig. 10(c). Note that although there are 16 magnon modes in total as a result of the 16 sublattices in the magnetic unit cell, owing to the collinear spin structure, the dynamical structure factors for the modes other than the two low-energy modes are negligible, as shown in Fig. 10(b).

The appearance of the symmetric shifts in the $+q$ and $-q$ directions for the antiferromagnetic magnons at first glance may suggest that these magnons are not nonreciprocal. Indeed, if one excites magnons with selected energy and momentum (or wavelength), two magnons propagating in the opposite directions will be simultaneously created. However, these two types of magnons in fact correspond to different spin dynamics, as confirmed by the in-field inelastic neutron scattering experiment, in which the two split branches of the antiferromagnetic magnons responded to the external magnetic field in the opposite fashion (Fig. 11), indicating the clockwise and counterclockwise nature of the two split modes. Hence, by exciting the system with not only a specific energy and momentum, but also a specific rotation direction, one can selectively create unidirectionally propagating magnons. The nonreciprocity of the antiferromagnetic magnons, thus, appears differently from that of the ferromagnetic magnons. This novel characteristic and its future prospects will be discussed in the next section.

5. Future Prospects

The nonreciprocal propagation of magnons in noncentrosymmetric ferromagnets has been of considerable interest recently because of the possible application for spintronics devices via the controllable propagation of the magnon spin current. In the past, however, the nonreciprocal magnon propagation in noncentrosymmetric ferromagnets was investigated using mostly microwave, optical, or electron scattering spectroscopy, owing to the stringent re-

quirement for the Q and $\hbar\omega$ resolutions as well as the magnetic field direction. As reviewed in this article, recent progress in the neutron inelastic scattering technique enables us to obtain the detailed momentum-dependent dispersion of the nonreciprocal magnons. While the polarized-neutron SANS technique can reveal the overall band shift of the ferromagnetic magnons in the vicinity of $\vec{Q} = 0$, small-angle inelastic scattering provides microscopic information of isotropic/anisotropic spin-spin interactions and anisotropies through the determination of the dispersion relation. Such an observation has only recently become possible. For the study of noncentrosymmetric ferromagnets, this technique will provide indispensable microscopic information, which has not been obtained by other means. Note further that small-angle inelastic scattering was made possible using a reactor-based cold-neutron triple-axis spectrometer, owing to its versatile flexibility for several experimental settings.

For noncentrosymmetric antiferromagnets, the present neutron scattering technique was found to be sufficient for the observation of magnon dispersion shifts, at least in α-$Cu_2V_2O_7$, where the extraordinarily large DM interaction brings about sizable splitting. Scientifically, on the other hand, the observation of magnon dispersion splitting in noncentrosymmetric antiferromagnets opens up many interesting topics for further research. By taking into account the nonlinear component originating from the asymmetric deformation of the magnon dispersion due to the DM interaction, Takashima *et al.* showed that a perfect nonreciprocal spin-Seebeck effect, where a spin current is allowed to propagate only in one direction regardless of the temperature gradient, is theoretically possible in α-$Cu_2V_2O_7$.[61] Even though the spin-Seebeck effect has been observed in α-$Cu_2V_2O_7$,[62] the nonreciprocity of the spin transport generated by a temperature gradient has not been experimentally confirmed. A future study to detect the nonreciprocity is of considerable interest, as this result may lead to a novel method to convert a temperature gradient to a macroscopic magnon spin current.

The double degeneracy of magnon bands in centrosymmetric antiferromagnets may be regarded as an internal degree of freedom of magnons in an analogy to the spin degree of freedom for electrons. On the basis of this analogy, Okuma[18] and Kawano *et al.*[19] proposed a possible "spin" texture around specific $\vec{k}$ positions, similar to the electron spin texture observed for the Rashba splitting, where spin-momentum locking gives rise to an intriguing vortex like texture. The linear crossing point in α-$Cu_2V_2O_7$ may be the simplest case of such spin-momentum locking, as the magnons in the upper band with $q > 0$ carry positive spins, whereas for $q < 0$, they carry negative spins. Designing the spin-momentum locking and consequently the "spin" texture for highly elaborate spin systems are at the forefront of research, and one may expect intriguing transport phenomena originating from such momentum-space

"spin" textures.

The rotation-direction sensitivity of the nonreciprocal magnon propagation has another interesting aspect proposed theoretically. The difference in phase velocities for magnons with different rotation directions (*i.e.*, clockwise and counterclockwise) will result in a spontaneous magnon birefringence effect. In contrast to the nonreciprocal magnons in ferromagnets, the net magnon spin current for antiferromagnets in thermal equilibrium is canceled out. However, the phase degree of freedom may propagate nonreciprocally even in thermal equilibrium in noncentrosymmetric antiferromagnets. It was further proposed that since the DM interaction, the existence of which is linked to the absence of local inversion symmetry, can be dependent on the electric polarization, the DM parameter may be controlled or varied by an external electric field.[63] As a result, the shift of the magnon dispersion may be tunable using an electric field, and hence an electric-field-induced magnonic Faraday effect has been proposed. The utilization of the phase degree of freedom of magnons, as was proposed in the above discussion, may lead to an intriguing new application for future devices based on the noncentrosymmetric antiferromagnetic magnons.

6. Conclusions

In this article, we have reviewed recent progress in the observation of the nonreciprocal magnons in noncentrosymmetric magnets, with particular attention to the inelastic neutron scattering results. In the prototypical noncentrosymmetric chiral magnet MnSi, the magnon dispersion relation was observed in the field-induced fully polarized (ferromagnetic) state. A unidirectional magnon dispersion shift was clearly observed in the experiment, consistent with earlier studies. It was further shown that the shift direction can be controlled by adjusting the bulk magnetization direction; this result opens a way to control the propagation direction of magnons using an external field. It is further commented that owing to the recent progress in the neutron scattering technique, it is now possible to obtain complementary information on the nonreciprocal magnon propagation to that obtained by the microwave or other $Q \sim 0$ techniques, which may be of significance for understanding and characterizing nonreciprocal ferromagnets for future device applications.

For noncentrosymmetric antiferromagnets, we have reviewed the recent observation of a bidirectional magnon dispersion shift in α-$Cu_2V_2O_7$. Such a magnon dispersion shift was expected in a recent theoretical study, and was for the first time confirmed in real materials using neutron inelastic scattering. It was further confirmed that the two split branches correspond to the spin dynamics with different directions of rotation; one rotates clockwise, whereas

the other rotates counterclockwise. This shifted magnon dispersion results in nonreciprocal propagation of phase degree of freedom even in the thermal equilibrium state, which opens a new way to realize magnon-based nonreciprocal flow. It was further mentioned that there are several theoretical proposals to utilize the antiferromagnetic magnons, such as an electric-field-induced magnonic Faraday effect, and hence it is of growing interest to investigate the potential of the magnons in noncentrosymmetric antiferromagnets for future applications in magnonic electronics.

Acknowledgments

The authors thank T. Arima for guiding us to this intriguing topic, T. Hong and Y. Zhao for continuous support in neutron experiments, Y. Motome for fruitful discussions, P. Piyawongwatthana for checking the spinwave calculations, and all our collaborators, D. Okuyama, A. Kikkawa, Y. Taguchi, Y. Tokura, G. Gitgeatpong, Y. Qiu, L. W. Harriger, and N. P. Butch, for various contributions. We also thank Y. Onose, S. Seki, and S. V. Gregoriev for their kind permissions to reproduce the figures. This work at IMRAM was partly supported by Grants-In-Aid for Scientific Research (Nos. 24224009 and 17K18744) from Japan Society for the Promotion of Science and by the research program "Dynamic alliance for open innovation bridging human, environment, and materials." KM is partly supported by the Thailand Research Fund Grant Number RSA6180081 and the Thailand Center of Excellence in Physics (ThEP). The stay of KM at IMRAM, Tohoku University, was supported by the "JSPS Invitational Fellowships for Research in Japan".

References

1) M. S. Dresselhaus, G. Dresselhaus, and A. Jorio, *Group Theory Applications to the Physics of Condensed Matter* (Springer-Verlag, Berlin, 2018).
2) E. I. Rashba, Sov. Phys. Solid State **2**, 1109 (1960).
3) Y. A. Bychkov and E. I. Rashba, JETP Lett. **39**, 78 (1984).
4) G. Bihlmayer, O. Rader, and R. Winkler, New J. Phys. **17**, 050202 (2015).
5) A. Manchon, H. C. Koo, J. Nitta, S. M. Frolov, and R. A. Duine, Nat. Mater. **14**, 871 (2015).
6) S. LaShell, B. A. McDougall, and E. Jensen, Phys. Rev. Lett. **77**, 3419 (1996).
7) J. Nitta, T. Akazaki, H. Takayanagi, and T. Enoki, Phys. Rev. Lett. **78**, 1335 (1997).
8) M. Z. Hasan and C. L. Kane, Rev. Mod. Phys. **82**, 3045 (2010).
9) N. P. Armitage, E. J. Mele, and A. Vishwanath, Rev. Mod. Phys. **90**, 015001 (2018).
10) N. Nagaosa, J. Sinova, S. Onoda, A. H. MacDonald, and N. P. Ong, Rev. Mod. Phys. **82**, 1539 (2010).
11) S. Itoh, Y. Endo, T. Yokoo, S. Ibuka, J.-G. Park, Y. Kaneko, K. S. Takahashi, Y. Tokura, and N. Nagaosa, Nat. Commun. **7**, 11788 (2016).
12) F.-Y. Li, Y.-D. Li, Y. B. Kim, L. Balents, Y. Yu, and G. Chen, Nat. Commun. **7**, 12691 (2016).
13) Y. Su, X. S. Wang, and X. R. Wang, Phys. Rev. B **95**, 224403 (2017).
14) S. A. Owerre, Phys. Rev. B **95**, 014422 (2017).
15) R. Chisnell, J. S. Helton, D. E. Freedman, D. K. Singh, R. I. Bewley, D. G. Nocera, and Y. S. Lee, Phys. Rev. Lett. **115**, 147201 (2015).
16) S. Bao, J. Wang, W. Wang, Z. Cai, S. Li, Z. Ma, D. Wang, K. Ran, Z.-Y. Dong, D. L. Abernathy, S.-L. Yu, X. Wan, J.-X. Li, and J. Wen, Nat. Commun. **9**, 2591 (2018).
17) S. Hayami, H. Kusunose, and Y. Motome, J. Phys. Soc. Jpn. **85**, 053705 (2016).
18) N. Okuma, Phys. Rev. Lett. **119**, 107205 (2017).
19) M. Kawano, Y. Onose, and C. Hotta, arXiv:1805.03925.
20) A. V. Chumak, V. I. Vasyuchka, A. A. Serga, and B. Hillebrands, Nat. Phys. **11**, 453 (2015).
21) R. Sasaki, Y. Nii, Y. Iguchi, and Y. Onose, Phys. Rev. B **95**, 020407(R) (2017).

22) G. L. J. A. Rikken and E. Raupach, Nature **390**, 493 (1997).

23) M. Kubota, T. Arima, Y. Kaneko, J. P. He, Y. Z. Yu, and Y. Tokura, Phys. Rev. Lett. **92**, 137401 (2004).

24) Y. Iguchi, S. Uemura, K. Ueno, and Y. Onose, Phys. Rev. B **92**, 184419 (2015).

25) S. Seki, Y. Okamura, K. Kondou, K. Shibata, M. Kubota, R. Takagi, F. Kagawa, M. Kawasaki, G. Tatara, Y. Otani, and Y. Tokura, Phys. Rev. B **93**, 235131 (2016).

26) R. Takagi, D. Morikawa, K. Karube, N. Kanazawa, K. Shibata, G. Tatara, Y. Tokunaga, T. Arima, Y. Taguchi, Y. Tokura, and S. Seki, Phys. Rev. B **95**, 220406(R) (2017).

27) Y. Tokura and N. Nagaosa, Nat. Commun. **9**, 3740 (2018).

28) R. L. Melcher, Phys. Rev. Lett. **30**, 125 (1973).

29) M. Kataoka, J. Phys. Soc. Jpn. **56**, 3635 (1987).

30) J. Fransson, A. M. Blak-Schaffer, and A. V. Balatsky, Phys. Rev. B **94**, 075401 (2016).

31) M. Garst, J. Waizner, and D. Grundler, J. Phys. D: Appl. Phys. **50**, 293002 (2017).

32) R. W. Damon and J. R. Eshbach, J. Phys. Chem. Solids **19**, 308 (1961).

33) L. K. Brundle and N. J. Freeman, Electron. Lett. **4**, 132 (1968).

34) T. An, V. I. Vasyuchka, K. Uchida, A. V. Chumak, K. Yamaguchi, K. Harii, J. Ohe, M. B. Jungfleisch, Y. Kajiwara, H. Adachi, B. Hillebrands, S. Maekawa, and E. Saitoh, Nat. Mater. **12**, 549 (2013).

35) K. Zakeri, Y. Zhang, J. Prokop, T.-H. Chuang, N. Sakr, W. X. Tang, and J. Kirschner, Phys. Rev. Lett. **104**, 137203 (2010).

36) K. Di, V. L. Zhang, H. S. Lim, S. C. Ng, M. H. Kuok, J. Yu, J. Yoon, X. Qiu, and H. Yang, Phys. Rev. Lett. **114**, 047201 (2015).

37) P. B. Braun, Nature **170**, 1123 (1952).

38) V. J. Folen, *Landolt-Bornstein Group III Condensed Matter* (Springer-Verlag, Berlin, 1970), Chap. 4b.

39) G. Meunier and M. Bertaud, J. Appl. Crystallogr. **9**, 364 (1976).

40) H. Effenberger and F. Pertlik, Monatsh. Chem. **117**, 887 (1986).

41) S. Seki, X. Z. Yu, S. Ishiwata, and Y. Tokura, Science **336**, 198 (2012).

42) S. Seki, M. Grast, J. Waizner, R. Takagi, Y. Okamura, K. Kondou, F. Kagawa, Y. Otani, and Y. Tokura, (submitted).

43) D. D. Stancil, *Theory of Magnetostatic Waves* (Springer, New York, 1993).

44) S. Mühlbauer, B. Binz, F. Jonietz, C. Pfleiderer, A. Rosch, A. Neubauer, R. Georgii, and P. Böni, Science **323**, 915 (2011).

45) Y. Ishikawa, K. Tajima, D. Bloch, and M. Roth, Solid State Commun. **19**, 525 (1976).

46) M. Ishida, Y. Endoh, S. Mitsuda, Y. Ishikawa, and M. Tanaka, J. Phys. Soc. Jpn. **54**, 2975 (1985).

47) Y. Ishikawa and M. Arai, J. Phys. Soc. Jpn. **53**, 2726 (1984).

48) G. Shirane, R. Cowley, C. Majkrzak, J. B. Sokoloff, B. Pagonis, C. H. Perry, and Y. Ishikawa, Phys. Rev. B **28**, 6251 (1983).

49) J. B. Sokoloff, W. H. Li, B. Pagonis, C. H. Perry, C. F. Majkrzak, G. Shirane, and Y. Ishikawa, Solid State Commun. **52**, 693 (1984).

50) S. V. Grigoriev, A. S. Sukhanov, E. V. Altynbaev, S. A. Siegfrid, A. Heinemann, P. Kizhe, and S. V. Maleyev, Phys. Rev. B **92**, 220415(R) (2015).

51) T. J. Sato, D. Okuyama, T. Hong, A. Kikkawa, Y. Taguchi, T.-H. Arima, and Y. Tokura, Phys. Rev. B **94**, 144420 (2016).

52) T. Weber, J. Waizner, G. S. Tucker, R. Georgii, M. Kugler, A. Bauer, C. Pfleiderer, M. Garst, and P. Böni, Phys. Rev. B **97**, 224403 (2018).

53) T. Weber, J. Waizner, G. S. Tucker, L. Beddrich, M. Skoulatos, R. Georgii, A. Bauer, C. Pfleiderer, M. Garst, and P. Boni, arXiv:1805.08750.

54) G. Gitgeatpong, Y. Zhao, P. Piyawongwatthana, Y. Qiu, L. W. Harriger, N. P. Butch, T. J. Sato, and K. Matan, Phys. Rev. Lett. **119**, 047201 (2017).

55) C. Calvo and R. Faggiani, Acta Crystallogr. Sect. B: Struct. Sci. **31**, 603 (1975).

56) P. Robinson, J. Hughes, and M. Malinconico, Am. Mineral. **72**, 397 (1987).

57) J. Pommer, V. Kataev, K.-Y. Choi, P. Lemmens, A. Ionescu, Y. Pashkevich, A. Freimuth, and G. Güntherodt, Phys. Rev. B **67**, 214410 (2003).

58) L. Ponomarenko, A. Vasil'ev, E. Antipov, and Y. Velikodny, Physica B **284-288**, 1459 (2000).

59) G. Gitgeatpong, Y. Zhao, M. Avdeev, R. O. Piltz, T. J. Sato, and K. Matan, Phys. Rev. B **92**, 024423 (2015).

60) G. Gitgeatpong, M. Suewattana, S. Zhang, A. Miyake, M. Tokunaga, P. Chanlert, N. Kurita, H. Tanaka, T. J. Sato, Y. Zhao, and K. Matan, Phys. Rev. B **95**, 245119 (2017).

61) R. Takashima, Y. Shiomi, and Y. Motome, Phys. Rev. B **98**, 020401 (2018).

62) Y. Shiomi, R. Takashima, D. Okuyama, G. Gitgeatpong, P. Piyawongwatthana, K. Matan, T. J. Sato, and E. Saitoh, Phys. Rev. B **96**, 180414 (2017).

63) R. Cheng, M. W. Daniels, J.-G. Zhu, and D. Xiao, Sci. Rep. **6**, 24223 (2016).